Contrib Mineral Petrol (2005) 150: 54–69
DOI 10.1007/s00410-005-0003-1

ORIGINAL PAPER

Yana Fedortchouk · Dante Canil · Jon A. Carlson

Dissolution forms in Lac de Gras diamonds and their relationship to the temperature and redox state of kimberlite magma

Received: 1 November 2004 / Accepted: 14 April 2005 / Published online: 20 July 2005

Abstract The degree and character of diamond dissolution were compared to crystallization temperatures (T) and oxygen fugacities (fO_2) estimated from chromite inclusions in olivine phenocrysts in several kimberlites from Lac de Gras, Northwest Territories, Canada. The T and fO_2 values calculated at an assumed pressure of 1 GPa are in the range of 970–1,140 ± 50°C and 2.8–4.4 log fO_2units below the nickel–nickel oxide (NNO) buffer. The T and fO_2 vary between kimberlites from northwest and southeastern clusters within 150°C and 1 log unit, respectively. A detailed description of morphological forms and surface dissolution features for diamond parcels from the Panda, Beartooth, Grizzly, Misery and Jay kimberlites (> 7000 stones) show that an increase in diamond resorption in the kimberlites corresponds to increase in T. The development of various surface dissolution pits and structures correlates with higher fO_2 of kimberlites and therefore mainly happens in the magma. The two processes of diamond dissolution, volume resorption and surface etching, do not show a strong correlation with each other, since some of the resorption occurs in the mantle. We suggest that the fO_2 of the kimberlite magma plays an important role in both the processes. The proportion of plastically deformed brown diamonds does not correlate with the degree of volume resorption, but does correlate with the development of surface forms. The diamond grade is higher in kimberlites with lower fO_2, confirming that conditions of kimberlite crystallization can have notable effect on diamond dissolution.

Electronic Supplementary Material Supplementary material is available for this article at http://dx.doi.org/10.1007/s00410-005-0003-1

Communicated by T.L. Grove

Y. Fedortchouk (✉) · D. Canil
School of Earth and Ocean Sciences, University of Victoria, Victoria, 3800 Finnerty Rd, BC V8W 3P6, Canada
E-mail: yana@uvic.ca
Tel.: +1-250-4724181
Fax: +1-250-7216200

J. A. Carlson
BHP Billiton Diamonds Inc, Kelowna, BC, Canada

Introduction

Natural diamonds recovered from kimberlites usually show a variety of morphological forms and surface features (Sunagawa 1984), reflecting the complex history of diamond growth, dissolution and transformation during its residence in the mantle and ascent in kimberlite melts. Diamond dissolution (resorption) can be a complex multi-stage process (Gurney et al. 2004) resulting in a variety of dissolution forms. Etch pits, ruts, corrosion sculptures, frosting and other surface features are commonly accepted to be the result of resorption and may lead to a very irregular form, and decrease in quality, of a diamond. For the formation of dodecahedra and tetrahexahedron (THH) diamond forms, two mechanisms, primary growth (Mendelssohn and Milledge 1995, and references therein) and resorption of octahedron stones (Robinson et al. 1989) were proposed. The latter is a commonly accepted mechanism supported by recent experimental studies of diamond dissolution that showed significant volume loss (Kozai and Arima 2003). Therefore, diamond resorption processes greatly influence the grade and value of diamonds in a kimberlite pipe.

High-temperature kimberlite magma is a reactive media for diamonds. Experimental studies on diamond dissolution in alkaline melts (Khokhryakov and Palyanov 1990; Kozai and Arima 2003; Sonin et al. 2002) have produced many of the resorption features observed in natural diamonds. Their results support the suggestion (Robinson et al. 1989) that the reaction with kimberlite is the main mechanism of diamond destruction. Resorption in the mantle was also documented (Gurney et al. 2004 and references therein).

Table 1 Geology, age, petrography and diamond grades for the Lac de Gras kimberlites used in the present study

Locality	Age (Ma)	Kimberlite geology	Matrix composition	Matrix minerals								Grade
				Carb	Ap	Mnt	Phl	Pv	Chr	Ti–Mt	Pyr	ct/t[f]
NW group												
Panda	53 ± 1[a]	Resedimented volcaniclastic kimberlite with minor primary volcaniclastic kimberlite[e]	Serp–Dol aggregate	P	P	–	–	P	P	P	–	0.95
Beartooth	53.1 ± 1[b]	–	–				–					1.2
Leslie	52.7 ± 2.9[b]	Mainly hypabyssal with a remnant of tuffistic kimberlite breccia (TKB)	Mnt grains in Serp matrix with Cc and Ap	P	P	P	P	?	P	P	–	0.33
Grizzly	50.8 ± 4.8[b]	Macrocrystic, heterolithic hypabyssal kimberlite	Mnt grains in Serp matrix	P	P	P	P	P	P	P	–	0.5
SE group												
Misery	–	Volcaniclastic kimberlite with associated dykes of macrocrystic hypabyssal kimberlite[e]	Serp–Cc aggregate with Ap& Phl	P	P	–	P	P	P	P	–	4.19
Jay	–	–	–			–						2.01
Central area												
Aaron	45.2 ± 1.3[b]											
Hypabyssal Aaron		Hypabyssal kimberlite	Mnt grains in Serp matrix with Cc	P	P	P	P	P	P	P	–	
Volcaniclastic		Pelletal volcaniclastic	Cc grains in Serp matrix	P	–	–	P	P	P	–	P	
Others												
Torrie	Late Cretaceous–early Paleocene[c]	Macrocrystic, heterolithic, volcaniclastic kimberlite tuff and tuff breccia	Cc grains in Serp matrix	P	M	–	M	–	P	P	P	
Ranch Lake	52.1 ± 0.3[d]	–	Cc grains in Serp matrix	P	–	?	P	–	P	–	P	0.2

The matrix phases are: Serp serpentine; Mnt monticellite; Cc calcite; Dol dolomite; Phl phlogopite; Pv perovskite; Chr chromite; Ti–Mt titano-magmetite; Pyr pyrite (P present, M minor, "–" absent)

[a]Based on Rb-Sr systematics on phlogopite macrocrysts (Gurney et al. 2004 and references therein)

[b]Based on Rb-Sr systematics on phlogopite macrocrysts (Creaser et al. 2004)

[c]From palynology (Nassichuk& McIntyre 1995).

[d]Lockhart et al. 2004

[e]From field guide to the Ekati Diamond Mine (materials for the 8th International Kimberlite conference)

[f]Diamond grades for Ekati pipes are from Natural Resources of Canada web-page, for Ranch Lake from Cookenboo (1996).

Experiments show that the mechanism for the diamond dissolution and resorption is oxidation by volatiles in kimberlite (CO_2 and H_2O) or components with variable valence states (e.g. Fe^{2+}–Fe^{3+}) where C is oxidized into CO_2 in the graphite stability field (Harris and Vance 1974; Arima 1998). Experiments on dissolution of diamond octahedrons in kimberlitic and lamproitic melts produced THH and dodecahedral forms where dissolution increased with temperature (T) and was suppressed by addition of CO_2 (Kozai and Arima 2003). The oxidation of diamonds in a gas flow greatly increases at higher fO_2 (Evans and Phaal 1961; Cull and Meyer 1986; Sonin et al. 2000). Furthermore, T and fO_2 were found to influence the orientation of trigon etch pits commonly observed on natural diamonds (Yamaoka et al. 1980) and the presence or absence of other etching forms (Sonin et al. 2002). The presence of water enhances the dissolution rate of diamond and causes a change in morphological forms from the formation of trigonal layers on flat-faced octahedrons (Chepurov et al. 1985; Pal'yanov et al. 1995) at dry conditions to ditrigonal layers in the presence of water. Thus, experimental studies have established the strong influence of intensive variables of kimberlite melt (T, fO_2, CO_2 and H_2O content) on the degree of diamond dissolution and the morphology of resorption forms.

At present, the characterization of mantle material entrained in kimberlites is the main tool for the prediction of grade and quality of diamonds in a pipe (Fipke et al. 1995). Since the properties of the host kimberlite influence the rate and character of diamond resorption, they may also be reflected in the characteristics of a diamond population. To test this idea, we compare the T and fO_2 of kimberlite melt crystallization with the diamond content and the character of resorption in diamonds from several well-characterized kimberlite pipes in the Lac de Gras region (NWT, Canada). Exceptionally, fresh kimberlites from the Lac de Gras region allowed us to apply olivine–spinel (Ol–Sp) thermometry and oxygen barometry (Ballhaus et al. 1991) to chromite inclusions in olivine phenocrysts in these kimberlites. Two clusters of kimberlites (northwest and southeast) in the Lac de Gras area differ in their degree of diamond resorption (Gurney et al. 2004). A detailed description of the morphology and surface features of individual stones was compiled for five kimberlite pipes from both clusters. One goal of the present study is to relate T–fO_2 data of kimberlite melts to different types of resorption and overall grade of the pipes in order to test as to what extent these parameters can be used in assessing the diamond potential of a pipe. A second objective is to establish what type of resorption coincides in time with the later stages of olivine phenocryst crystallization.

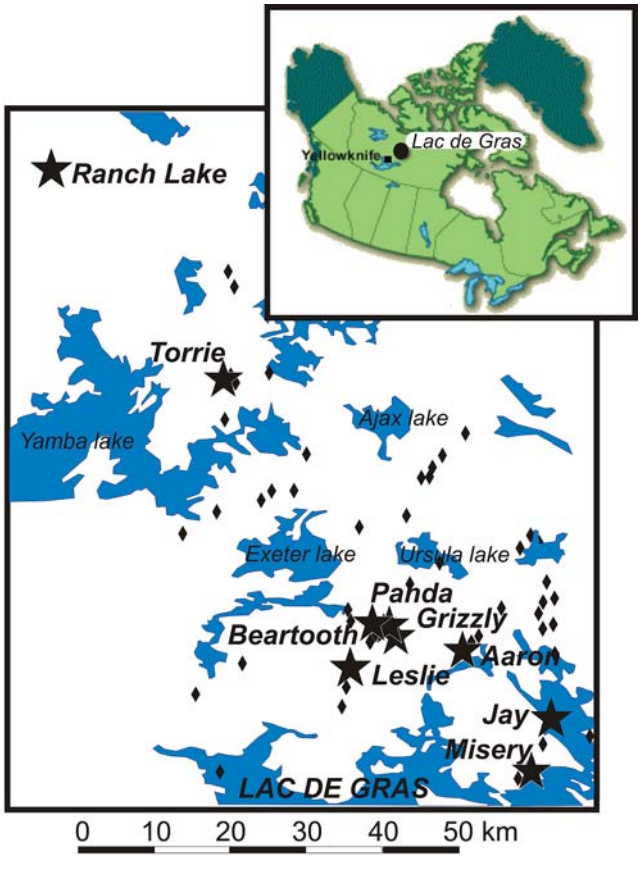

Fig. 1 Location of kimberlite pipes (*black diamonds*) in the Lac de Gras kimberlite field, NWT, Canada. The kimberlites used in the present study are shown with *black stars*

Geological background

The Lac de Gras kimberlites were emplaced in Archean rocks of the east-central part of the Slave Province, Canada (Davis and Kjarsgaard 1997; Pell 1997; Creaser et al. 2004) and are subdivided according to their age

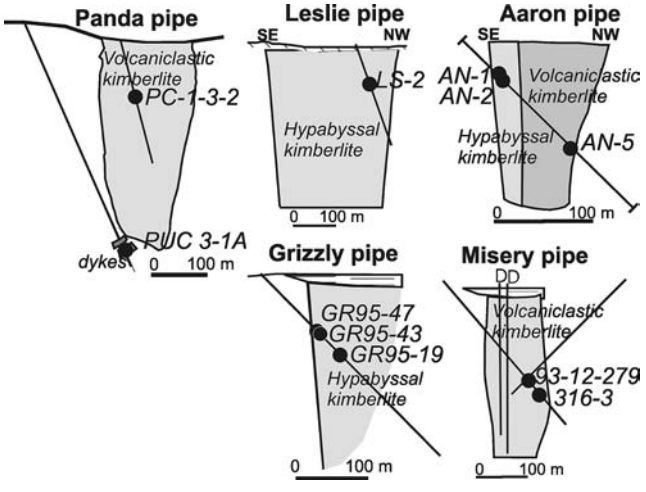

Fig. 2 Cross-sections of the Panda, Leslie, Aaron, Grizzly and Misery kimberlite pipes with the location of samples used in this study are shown. In the Misery pipe the diamonds described in this study were recovered from two drill holes "D"

and spatial distribution into northwest (~53 Ma), southeast (~56 Ma) and central clusters (~48 Ma) (Gurney et al. 2004). Thermobarometric data was obtained for eight kimberlite pipes that fall within all three clusters (Table 1, Fig.1). The diamond populations from five of these pipes, Panda, Misery, Beartooth, Grizzly and Jay, were described in terms of their morphology and presence of various resorption features. The Ranch Lake kimberlite may represent an extension of the NW group (Lockhart et al. 2004).

The composition and petrography of the nine kimberlites from this study are summarized in Table 1. Hypabyssal facies kimberlites contain fresh phenocrysts of olivine (0.2–1 mm) without any notable alteration. In volcaniclastic facies only margins of olivine are serpentinized. The matrix of hypabyssal kimberlite contains abundant monticellite (up to 80 μm) surrounded by a fine-grained aggregate of serpentine and calcite. Monticellite is absent in the matrix of volcaniclastic facies that consist of serpentine-calcite aggregate with numerous calcite grains (up to 100 μm) precipitated from a fluid phase.

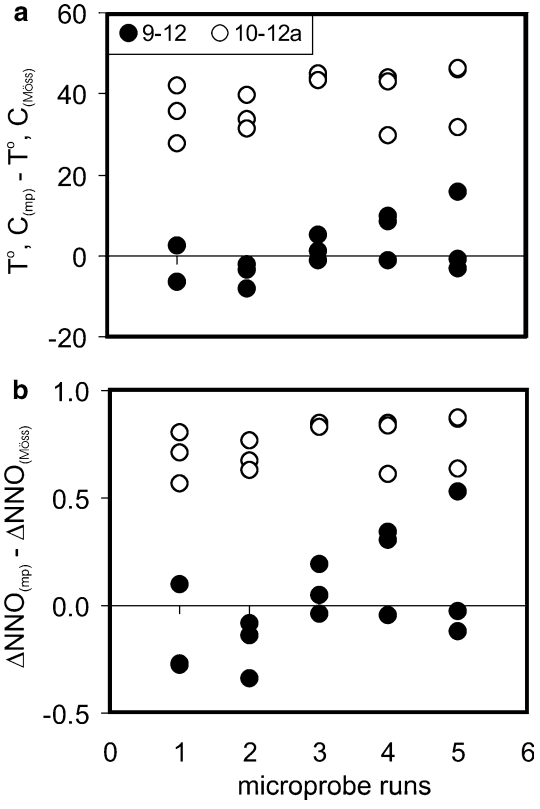

Fig. 3 T–fO_2 data obtained for two chromites with Fe^{3+} known from Mössbauer spectroscopy (McCammon and Kopylova, 2004). The plots show differences in the **a** calculated temperature, and **b** fO_2 (expressed as Δ NNO) using microprobe data and Mössbauer spectroscopy data for Fe^{3+} in the two chromite grains

Methods

Sample selection and thermobarometry

The kimberlite samples we selected for the T–fO_2 calculations represent the main kimberlite body for the pipes having a complex structure (Fig.2). For the Panda and Misery pipes, however, kimberlite dykes were also studied. Both volcaniclastic and hypabyssal facies samples were collected for the Aaron pipe.

Olivine phenocrysts in both hypabyssal and volcaniclastic facies contain inclusions of euhedral (5–10 μm) aluminous magnesian chromites. The chromites occur in the margins of olivine phenocrysts and therefore record the conditions in kimberlite magma at the end of the phenocryst crystallization. For olivine–spinel assemblages the reaction:

$$\underset{\text{Olivine}}{6Fe_2SiO_4} + O_2 = \underset{\text{Orthopyroxene}}{3Fe_2Si_2O_6} + \underset{\text{Chromite}}{2Fe_3O_4} \quad (1)$$

was used as an oxygen barometer and $FeMg_{-1}$ exchange thermometer ($T_{Ol\text{-}Sp}$) (O'Neill and Wall 1987; Ballhaus et al. 1991) . Microprobe data for both minerals were used in the calculations and the uncertainties of this approach are described in detail in the electronic supplementary material (ESM) Appendix. The uncertainty in T–fO_2 calculations from the Fe^{3+} /Σ Fe of chromites determined from the microprobe data was evaluated using secondary standards (Wood and Virgo 1989) (Fig. 3). The log fO_2 values calculated from the Ol–Sp oxygen barometer are maxima and require a correction for the low silica activity of kimberlite melts (Fedortchouk and Canil 2004). The maximum silica activity is limited by the presence of monticellite that crystallizes following the Ol–Sp assemblage, as observed petrographically and by experiment in kimberlite (Edgar et al. 1988). The silica activity in kimberlite must lie below the reaction:

$$CaMgSi_2O_6 = SiO_2 + CaMgSiO_4$$

The lower silica activity of kimberlite magmas, relative to the Ballhaus et al. (1991) calibration, results in lower calculated fO_2 values. A minima in calculated fO_2, however, and thus in silica activity, is limited by the lack of FeNi metal (i.e. the Ni precipitation curve—O'Neill and Wall 1987) in kimberlite olivines we studied. The criteria for the selection of olivine and chromite grains suitable for these calculations, the applicability of Ol–Sp thermobarometry for this assemblage and further details of the calculation at variable Si activity in the melt are described at length elsewhere (Fedortchouk and Canil 2004). The lack of knowledge of the exact silica activity affects the absolute accuracy of our fO_2 estimates, but our study mainly concerns relative differences in fO_2 between pipes, and the precision in the measurements ensures that such differences are real (Fig. 3 and ESM Appendix).

Diamond descriptions

Diamond parcels from the Panda, Beartooth, Misery, Grizzly, and Jay kimberlites (>1,500 carats, >26,000 stones) were recovered from reverse circulation drill holes collared within each pipe. The parcels were sieved into nine classes using Tyler sieves (square mesh). The diamonds range from approximately 4 carats to less than 0.001 carat (sieve size of +3.5 to −25 mm or +9 mm to −710 μm, respectively). For the sieve classes with less than 200 stones, all diamonds were individually described. The larger populations were randomly split and approximately 25–50% of the stones (at least 100 from each group) were described. To ensure that this

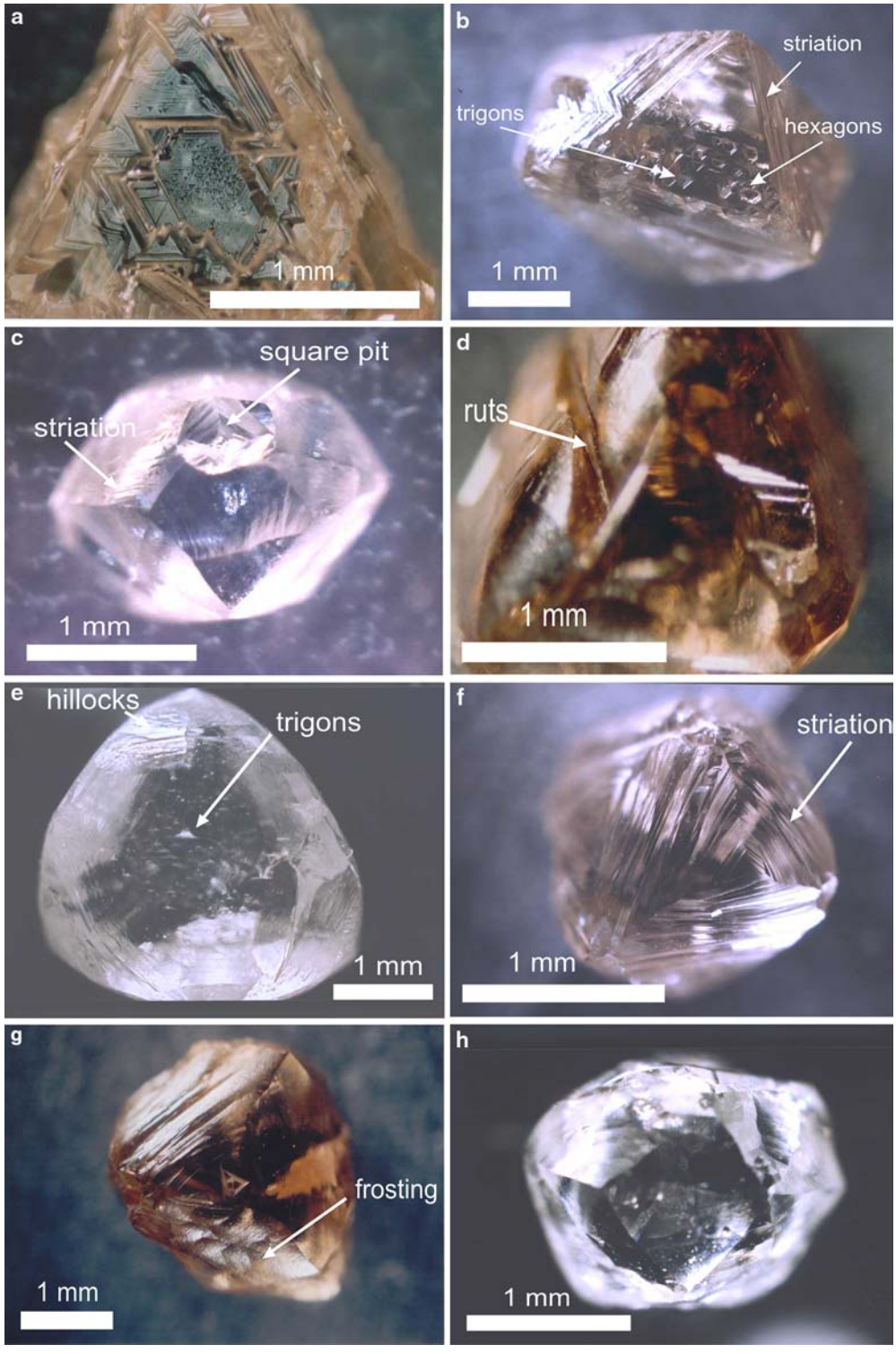

Fig. 4 Examples of surface features in Lac de Gras diamonds used in this study: **a** Macle diamond with two types of trigon etch pits—larger earlier trigons, and smaller later trigons. **b** Octahedral diamond with trigon and hexagon etch pits developed on face (111) and striation in the direction (110). **c** THH diamond with square pits developed on face (110) and striation. **d** Rut on a resorbed octahedron diamond. **e** Resorbed macle with hillocks and trigon pits. **f** THH diamond with striation. **g** Frosted surface of a resorbed octahedral diamond. **h** Glossy surface of THH diamond without any visible surface features

approach produces representative diamond populations, we extended the description of a few sieve classes from Panda to a larger number of diamonds and found no influence on the results. In total over 7,000 stones (almost 1,000 carats) were individually described.

The physical properties recorded in the diamonds include weight, colour, colour intensity, crystal morphology, presence of internal fractures and inclusions, surface growth and dissolution features. A more detailed description scheme exists (Gurney et al. 2004), but only the influence of resorption processes on crystal morphology and development of etch features are addressed in this study. To collect information from the larger number of stones, we used an optical microscope for the observation of the diamond surface features. Therefore, resorption events forming the smallest etch pits may not be reflected in our data.

The classification of crystal morphology was simplified into four major forms: octahedron and cube (primary forms), tetrahexahedroid (THH) (secondary form) and irregular broken stones. For the purpose of this study, we did not distinguish between two products of octahedron resorption: dodecahedron and THH. We recorded the degree of resorption, however, as the percentage of the octahedral faces dissolved. We divided octahedrons into three groups according to percentage resorption of octahedral faces: (1) 0%, (2) $<25\%$, (3) 25–50%. THH was classified as a stone with more than 50% resorption. The degree of resorption was recorded only for octahedron–THH crystal morphologies. The evolution of cube morphology with resorption is not well understood, but cubes are only a minor portion of the diamond populations from kimberlites we studied.

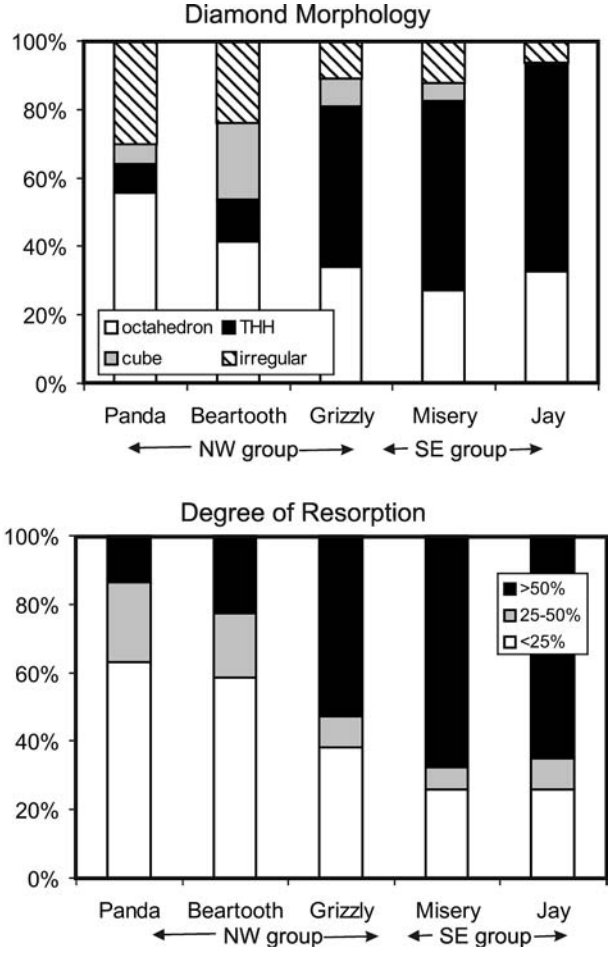

Fig. 5 **a** Distribution of major morphological forms of diamond, and **b** proportion of variously resorbed octahedral diamonds in the Panda, Beartooth, Grizzly, Misery and Jay kimberlites. Percents show the percentage resorption of octahedral faces. The plot shows the higher resorption for diamonds from the SE cluster of kimberlites

Results

Resorption in Lac de Gras diamonds

Natural stones often show several growth zones where some dissolution may have occurred between different growth events and conditions (Taylor et al. 1995). Dissolution may change the morphology of the diamond to produce a variety of crystal forms with various combinations of octahedron and THH faces, and may develop etch pits, ruts, hillocks, striation, disks, frosting, and corrosion structures on the diamond surface (Robinson et al. 1989). The presence of etch pits depend on the conditions of the etching and the diamond morphology: trigons form on (111) and squares on (100) faces. They often show few generations from the earlier large pits to the later small ones (Fig. 4a).

For our purpose we combined all of the observed dissolution features into two major groups. The first, resorption, refers to the development of secondary THH faces on the octahedral crystals that may be accompanied with a substantial loss of volume. The degree of resorption is described as a ratio of octahedron to THH (O/THH). The second, etching or surface features, describes all the diverse surface structures produced by the dissolution processes.

Resorption

The diamond populations of kimberlites from different clusters within the Lac de Gras area have the same diamond types in terms of their morphology and colour, but the proportion of these types differ significantly between the clusters (Gurney et al. 2004). The degree of resorption is very low in Panda and Beartooth diamonds (NW cluster) which are dominated by mainly colourless flat-faced octahedrons (Fig. 5a, Tables 2, 3). In contrast, diamonds from Misery and Jay (SE cluster) are highly resorbed (Fig. 5b) with a very high proportion of THH and brown stones (Fig. 5a, Tables 2, 3). The Grizzly population is drastically different from the other NW kimberlites by having a very high proportion of brown stones and resorbed THH forms.

Table 2 Morphology of diamonds from the five Lac de Gras kimberlites

Locality	NW group			SE group	
	Panda	Beartooth	Grizzly	Misery	Jay
Octahedron	1,693	1,107	427	4,595	960
THH	259	328	592	9,364	1,759
Cube	176	596	104	851	18
Irregular	918	635	139	2,100	193
Other forms[a]	17	7			
Total stones	3,047	2,667	1,279	16,909	2,936
O/THH	6.5	3.4	0.7	0.5	0.5

[a]Other forms (cubo–octahedrons, cubo–THH, laminar dodecahedrons etc.) were recorded only in the Grizzly and Jay diamond parcel

Table 3 Degree of resorption in octahedron diamonds from the five Lac de Gras kimberlites present as per cent of octahedron faces resorbed (0%, no resorption; and > 50%, THH)

Locality	NW group			SE group	
	Panda	Beartooth	Grizzly	Misery	Jay
0%	164	67	200	2,017	415
< 25%	971	757	227	1,588	290
25–50%	422	261	98	895	245
> 50%	245	320	590	9,367	1,766
Total	1,803	1,404	1,116	13,965	2,758

Main types of surface features on Lac de Gras diamonds

The terminology for the description of diamond surface features in this study is based on previous work (Robinson et al. 1989; Afanasiev et al. 2000).

Table 4 Presence of various surface features (resorption and growth) in octahedron and THH diamonds from the five Lac de Gras kimberlites

Locality	NW group			SE group	
	Panda	Beartooth	Grizzly	Misery	Jay
Octahedrons					
Trigons	1,178	742	197	920	318
Hexagons	21	16	30	46	9
Ruts	726	302	36	296	74
Frosting	90	32	183	439	173
Step faces	302	184	206	2,145	476
No etching	322	315	167	3,217	473
Total	1,702	1,107	427	4,573	984
THH					
Trigons	60	105	82	571	86
Squares	5	0	37	276	58
Hillocks	0	4	28	2,036	105
Striation[a]	ND	ND	179	ND	606
Ruts	99	76	82	2,432	198
Frosting	7	9	461	4,552	1,260
No etching	89	182	249	4,750	874
Total	206	328	587	9,325	1,775

[a]Striation was present in all the pipes, but was described only in the Grizzly and Jay

Etch pits (trigons, hexagons, squares). Negatively oriented trigon pits (Fig. 4b) developed on (111) face of octahedrons are very common on the Lac de Gras diamonds. In rare cases they develop into hexagons. Square pits are less common than trigons and appear on THH faces in the (100) direction (Fig. 4c). Positively oriented trigons are usually too small to be seen under the optical microscope and therefore were not recorded in the present study.

Ruts are slots and etch channels present in all types of diamonds (Fig. 4d). They form after fractures and, therefore, depend not only on the intensity of the dissolution processes but also on the presence of cracks on the diamond surface. Nevertheless, the kimberlites with a higher proportion of rutted diamonds underwent more extensive dissolution.

Hillocks (Fig. 4e) are irregularities of pyramid shape, drop-shape or elongate shape and are common on THH faces.

Striations (Fig. 4f) are common features on THH and along the edges of resorbed octahedrons from all the pipes, but were recorded only in Grizzly and Jay stones, and include different types of lamination and stepped patterns. It is not always possible to distinguish between the growth and dissolution forms. Step faces on the octahedrons were assigned to growth if they have sharp edges, whereas those with rounded corners and curved edges were considered as secondary forms.

Frosting (Fig. 4g) is believed to form in near-surface conditions (Afanasiev et al. 2000) and therefore is not a focus of our study. We recorded the presence of frosting, but did not distinguish between its coarse and fine types.

There is a proportion of octahedral and THH diamonds in all the pipes that do not show any traces of dissolution and have glossy surfaces (Fig. 4h).

The presence of different types of surface dissolution features in octahedron and THH stones from the five Lac de Gras pipes are given in Table 4 and on Fig. 6. The main forms are various etch pits and ruts that show similar distribution patterns between the pipes, indicating that they may be formed by the same process. Etch pits and ruts are present on the larger proportion of stones from the Panda and Beartooth and notably less so in Misery and Jay. Frosting is a very common feature in octahedrons and THH from Grizzly and in THH from Misery and Jay. In general, surface etching is more common in Panda and Beartooth and less in Misery and Jay kimberlites.

T- fO_2 calculations for Lac de Gras kimberlites

In the present study we expanded previous T and fO_2 calculations (Fedortchouk and Canil 2004) to a larger number of pipes where the diamond data is available. We can also compare the crystallization conditions of kimberlites from different clusters (Table 5, Fig. 7).

Oxygen fugacity and crystallization temperatures obtained for the eight Lac de Gras kimberlites form

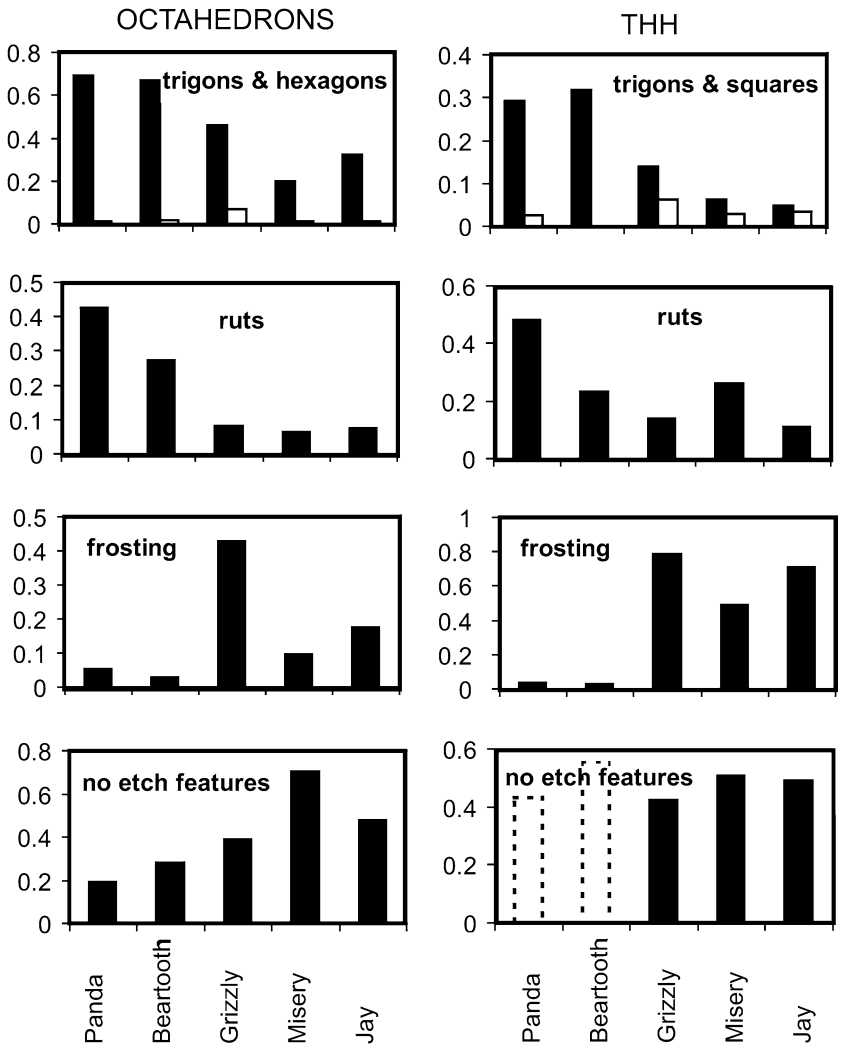

Fig. 6 Proportions of stones with various surface features in octahedral and THH diamonds from the Panda, Beartooth, Grizzly, Misery and Jay kimberlites. Trigons are shown as *black boxes*, hexagons and squares as *white boxes*. The proportion of THH diamonds without etch features in Panda and Beartooth are shown as *dash lines* because the diamond descriptions for these parcels lack information on the presence of striations

distinctive separate trends for each pipe (Fig. 7a). They show that during co-crystallization of Ol–Sp assemblage, the melt became more reduced relative to the NNO buffer. The fO_2 evolution with T in the kimberlites is approximately parallel to Wustite–Magnetite (WM) buffer and therefore the differences in fO_2 between different kimberlite bodies is more obvious when viewed relative to the WM buffer to eliminate the T effect (Fig. 7b). A decrease in fO_2 during groundmass crystallization in kimberlites was also described at temperatures below 800°C (Mitchell 1986).

As noted above, the silica activity of the kimberlites are somewhere below that of the Diopside Monticellite (Di–Mnt) buffer and the fO_2 values shown on Fig. 7 are therefore maximum values. The minimum fO_2values are limited by the lack of any native metal to be slightly above the Ni precipitation curve just above the IW buffer (O'Neill and Wall 1987). Thus, log fO_2 of the kimberlites could be in the range −11.5 to −13 at 1,100°C and an assumed pressure of 1 GPa. The uncertainties of our fO_2 calculations are smaller than this range of fO_2 (Fig. 3 and ESM Appendix). We do not know the pressure of Ol–Sp co-crystallization, but for the range of possible pressures under which monticellite is stable in these kimberlites (0.1–1 GPa, Fedortchouk and Canil 2004), the effect of P is 20°C/GPa on $T_{\text{Ol-Sp}}$, 0.14 log unit/GPa on silica activity, and 0.4 log unit/GPa on fO_2 .

The margins of olivine phenocrysts from all the kimberlites have uniform composition of Mg# (Mg/Mg+ Fe) 0.91–0.92 (ESM Table 1). Olivines from the Torrie and Ranch Lake pipes have slightly lower and higher Mg#, respectively, than phenocrysts from the seven other pipes. The variations in calculated T and fO_2, however, are mainly determined by the variation in chromite composition. The inclusions in olivine phenocrysts are titanian aluminous magnesian chromites (according to Mitchell 1986), with a positive correlation between Cr/Cr + Al (0.6–0.9) and $Fe^{2+}/Fe^{2+} + Mg$ (0.3–0.5) corresponding to the macrocrystal trend of Mitchell (Mitchell 1986), but TiO_2 (1–4 wt%) of the Lac de Gras chromites are slightly higher (Table 2). Variations in the chromite composition between different kimberlites are most distinctive in terms of the Cr- and

Table 5 Equilibrium temperatures and oxygen fugacities calculated for Leslie, Aaron, Grizzly, Torrie, Panda, Beartooth, Misery and Ranch Lake kimberlites by Ol–Sp thermobarometery at an assumed pressure of 1 Gpa

Sample	Ol–Sp, T (°C)[a]	$\Delta\log fO_2^{FMQ}$ [b]	$\log a^{c}_{SiO2}$		Corrected[d]		
			Di-Mont	En-Fo	$\log fO_2$	ΔNNO	ΔWM
Panda kimberlite							
PC132-2	1,069	1.1	−1.68	−0.54	−11.7	−2.7	−0.9
PC132-16	1,059	1.1	−1.70	−0.54	−11.9	−2.8	−0.9
PC132-19	1,040	1.0	−1.73	−0.55	−12.3	−3.0	−1.0
PC132-24	1,074	0.9	−1.68	−0.54	−11.9	−3.0	−1.2
PC132-26	1,086	1.2	−1.65	−0.53	−11.4	−2.6	−0.9
PC132-31	1,058	1.1	−1.70	−0.54	−11.9	−2.8	−0.9
PC132-32	1,057	0.8	−1.70	−0.54	−12.2	−3.1	−1.2
PC131-1	1,016	1.0	−1.78	−0.57	−12.8	−3.1	−1.0
Panda dyke							
puc31A-4	1,021	1.0	−1.77	−0.57	−12.7	−3.0	−1.0
puc31A-5	1,052	1.2	−1.71	−0.55	−11.9	−2.7	−0.8
puc31A-6	967	1.7	−1.87	−0.60	−13.0	−2.5	−0.2
puc31A-7	1,037	1.2	−1.74	−0.56	−12.2	−2.8	−0.8
Beartooth kimberlite							
BDC11-264-4	1,036	0.9	−1.74	−0.56	−12.5	−3.1	−1.1
BDC01-179.8-1	1026	1.0	−1.76	−0.56	−12.6	−3.0	−0.9
BDC01-179.8-2	1024	1.0	−1.76	−0.56	−12.7	−3.1	−1.0
BDC-01-159.8-2	1,018	1.1	−1.77	−0.57	−12.6	−2.9	−0.9
BDC-01-158.1-2	1,032	1.1	−1.75	−0.56	−12.4	−2.9	−0.9
Misery kimberlite							
316-3-1 dyke	1,066	1.0	−1.69	−0.54	−11.9	−2.8	−1.0
316-3-1rim dyke	1,053	1.2	−1.71	−0.55	−12.0	−2.8	−0.9
93-12-279-1	1,138	0.8	−1.57	−0.50	−10.9	−2.8	−1.2
93-12-279-2	1138	0.8	−1.57	−0.50	−10.9	−2.8	−1.3
93-12-279-3	1,137	0.7	−1.57	−0.50	−11.0	−2.9	−1.4
93-12-279-4	1,125	0.8	−1.59	−0.51	−11.1	−2.8	−1.3
93-12-279-5	1,112	0.8	−1.61	−0.51	−11.4	−3.0	−1.3
93-12-279-6	1,089	0.8	−1.65	−0.53	−11.7	−3.0	−1.3
93-12-279-7	1,112	0.8	−1.61	−0.51	−11.3	−2.9	−1.3
93-12-279-3	1,069	0.7	−1.68	−0.54	−12.2	−3.2	−1.3
93-12-279-8	1,091	0.7	−1.65	−0.53	−11.8	−3.1	−1.3
Leslie kimberlite							
LS2-k-2	1,049	1.1	−1.72	−0.55	−12.1	−2.8	−0.9
LS2-m-1b	1,044	1.1	−1.73	−0.55	−12.2	−2.9	−0.9
LS2-m-2	1,031	1.1	−1.75	−0.56	−12.4	−2.9	−0.8
Ls2-n	1,101	1.3	−1.63	−0.52	−11.0	−2.5	−0.8
Aaron kimberlite							
AN2-8	999	1.1	−1.81	−0.58	−13.0	−3.1	−0.9
AN2-16	1,052	0.9	−1.71	−0.55	−12.2	−3.0	−1.1
AN5-b-1	1,084	1.1	−1.66	−0.53	−11.5	−2.7	−1.0
AN5-c-2	1,053	0.9	−1.71	−0.55	−12.2	−3.0	−1.1
An1-l	1,071	1.0	−1.68	−0.54	−11.8	−2.9	−1.1
An1-k	1,073	1.0	−1.68	−0.54	−11.8	−2.8	−1.0
Grizzly kimberlite							
GR95-47-1	1,078	1.1	−1.67	−0.53	−11.6	−2.7	−0.9
GR95-47-5	1,052	1.1	−1.71	−0.55	−12.0	−2.8	−0.9
GR95-47-13	1,015	1.0	−1.78	−0.57	−12.8	−3.0	−1.0
GR95-47-13	1,021	1.0	−1.77	−0.57	−12.7	−3.0	−1.0
GR95-47-14	1,065	0.8	−1.69	−0.54	−12.2	−3.1	−1.3
GR95-47-24	1,088	1.2	−1.65	−0.53	−11.4	−2.6	−0.9
GR95-47-25	1,080	1.1	−1.66	−0.53	−11.5	−2.7	−0.9
GR95-47-25	1,075	1.1	−1.67	−0.53	−11.7	−2.8	−0.9
GR95-47-26	1,106	0.9	−1.62	−0.52	−11.3	−2.8	−1.1
GR95-47-27	1,063	1.0	−1.69	−0.54	−11.9	−2.9	−1.0
GR95-43-k2	1,085	1.2	−1.66	−0.53	−11.4	−2.7	−0.9
GR95-43-e	1,115	1.2	−1.61	−0.51	−10.9	−2.5	−0.9
GR95-43-a1	1,099	0.9	−1.63	−0.52	−11.5	−2.9	−1.2
Torrie kimberlite							
TQ94-17-13-10	1,111	1.0	−1.61	−0.51	−11.1	−2.7	−1.0
TQ-18E-2	1,080	1.3	−1.66	−0.53	−11.4	−2.6	−0.8
TQ13-h-1	1,067	0.8	−1.69	−0.54	−12.1	−3.1	−1.2
TQ17-f-1	1,140	1.3	−1.57	−0.50	−10.4	−2.3	−0.8
Ranch Lake kimberlite							
RL1-3	1,098	1.5	−1.63	−0.52	−10.9	−2.3	−0.6

Table 5 (Contd.)

Sample	Ol–Sp, T (°C)[a]	$\Delta\log fO_2^{FMQ}$ [b]	$\log a_{SiO2}^{c}$		Corrected[d]		
			Di-Mont	En-Fo	$\log fO_2$	ΔNNO	ΔWM
RL3-2	1053	1.5	−1.71	−0.55	−11.6	−2.4	−0.5
RL3-5	1,130	1.0	−1.58	−0.50	−10.9	−2.7	−1.1
RL3-6	1,061	1.5	−1.70	−0.54	−11.5	−2.4	−0.5
RL3-12	1,085	1.6	−1.66	−0.53	−11.0	−2.2	−0.4
RL2-1	1,078	1.3	−1.67	−0.53	−11.4	−2.6	−0.4

[a]Temperatures calculated from FeMg_1 Ol–Sp thermometer. See Ballhaus et al. (1991) and O'Neill and Wall (1987)
[b]Oxygen fugacities at 1 GPa calculated relative to FMQ buffer with oxygen barometer by Ballhaus et al. (1991)
[c]Silica activity of Diopside–Monticellite (Di–Mont) and Enstatite–Forsterite (En–Fo) buffers calculated using thermodynamic data of Holland and Powell (1998)
[d]Corrected maximum values of oxygen fugacities in kimberlites calculated for silica activity of Diopside–Monticellite buffer. Equation for NNO buffer is from Ballhaus et al. (1991 and references therein) and for WM buffer is from Frost (1991)

Ti-content (Fig. 8). In the Torrie kimberlite, Mg# is low in both the mineral phases and probably indicates the higher Fe-content of its melt. The high TiO_2 of the Torrie chromites and presence of other Ti-bearing phases (ilmenite and rutile) suggest that the Torrie kimberlite melt was probably enriched in Ti compared to the other magmas.

Discussion

Variations in T and fO_2 of kimberlites

The precision of the T and fO_2 calculations (Fig. 3 and ESM Appendix) permits an examination of the *relative* differences between the kimberlites. The T and fO_2 values of the Ekati kimberlites correlate with their division by age and location into clusters. The fO_2 decreases and crystallization T slightly increases from the NW cluster (Panda, Beartooth and Leslie kimberlites) to the Central zone (Aaron) and further to the SE cluster (Misery) (Fig. 9). The Grizzly kimberlite has two T–fO_2 trends, one between the NW cluster and the Aaron pipe, and another closer to the Misery pipe (Fig. 7b). The Grizzly pipe is geographically part of the NW group (Fig. 1), but its age estimation has larger uncertainties and it may be as young as the Central zone pipes (Table 1). Both T–fO_2 trends in the Grizzly pipe have similar chromite compositions. The differences in fO_2 are due to the low Mg of the olivines crystallized at lower fO_2. These olivines also have higher CaO contents. This variation in T–fO_2 data within the Grizzly pipe may be due to some local effect within the kimberlite or perhaps the mixing of different magmas.

Variations between all the kimberlites are within 150°C and 1 log fO_2 unit. The fO_2 variation between the kimberlite melts may be due to the differences in the redox regime of their mantle source or produced during ascent and crystallization of the melts. In the first case, the increase in fO_2 of the mantle source would be lateral from SE to NW or fluctuate with time (Table 1, Fig. 9). In the second case, the original fO_2 of the melts could diverge due to differences in their degassing history, mixing with other magmas or entrainment of different xenolithic material. Differences in the crystallization path are unlikely, given the similarities in mineral assemblages of all the kimberlites.

Influence of magma crystallization conditions on diamond populations

Substantial differences in the appearance and quality of diamonds between the NW and SE kimberlite clusters in the Lac de Gras field were revealed by Gurney et al. (2004). A significant increase in resorption and in the proportion of brown stones from the NW group (Panda, Beartooth, Leslie) to the SE group (Misery, Jay) was observed. The Grizzly diamonds differ greatly from the other NW kimberlites by having a much higher proportion of brown stones and substantial resorption. Gurney et al. (2004) explored how local events in the mantle and variations in sampling of different mantle domains by kimberlite magmas could produce the observed differences in the diamond populations. In a complementary way, we focus instead on the surface features and morphology of diamonds to see how they may correlate with the properties of the host kimberlite melt.

A significant effect of T and fO_2 on the rate of diamond dissolution was demonstrated by experiment (Sonin et al. 2000; Kozai and Arima 2003). Our data shows a general correlation between the characteristics of the diamond population and the T and fO_2 of the host kimberlite. Increases in the degree of resorption for diamonds from Panda and Beartooth to Misery and Jay (Fig. 5a, b) correlate with an increase in crystallization T (Fig. 7b). The more extensive development of surface etch features in Panda and Beartooth diamonds correlates with their higher oxidation state (Fig. 7b). The Grizzly diamonds are notably different from the other NW kimberlites and have much larger T and fO_2 variation than the other pipes from the NW cluster.

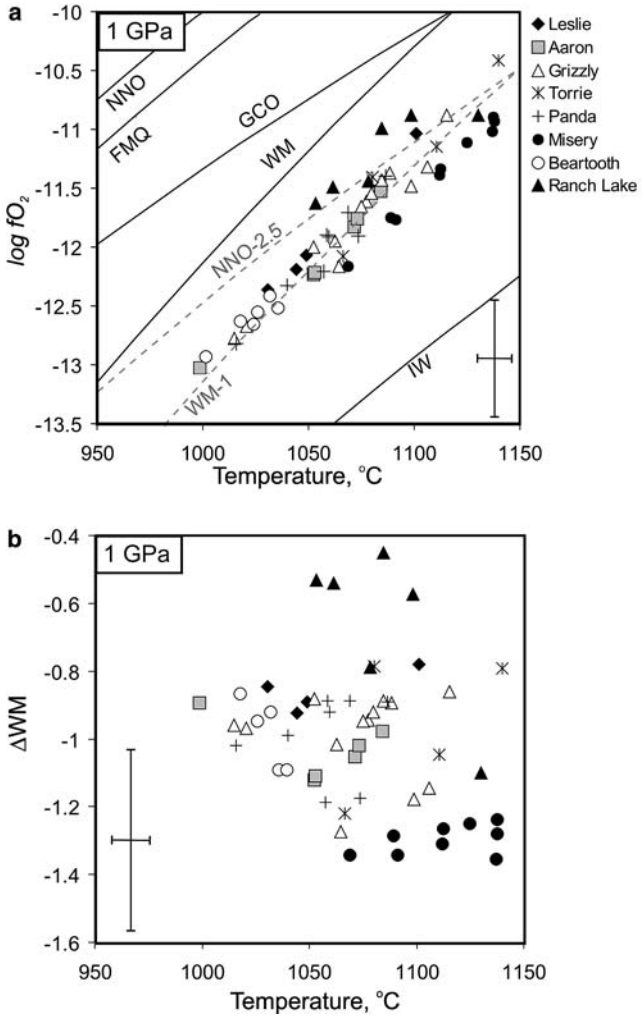

Fig. 7 **a** Crystallization T and log fO_2 calculated from Ol–Sp thermometry and oxybarometry (Ballhaus et al. 1991) for eight Lac de Gras kimberlites compared to different oxygen buffers; fayalite–magnetite quartz (FMQ) and nickel–nickel oxide (NNO), wustite–magnetite (WM) and iron–wustite (IW) (O'Neill and Wall 1987; Frost 1991). The individual trends in each kimberlite is approximately parallel to the WM buffer and the relative differences between the kimberlites can best be seen relative to this buffer (**b**). Plot shows how the variations in T and fO_2 between the different kimberlites are larger than the precision of the method (shown as *error bars*)

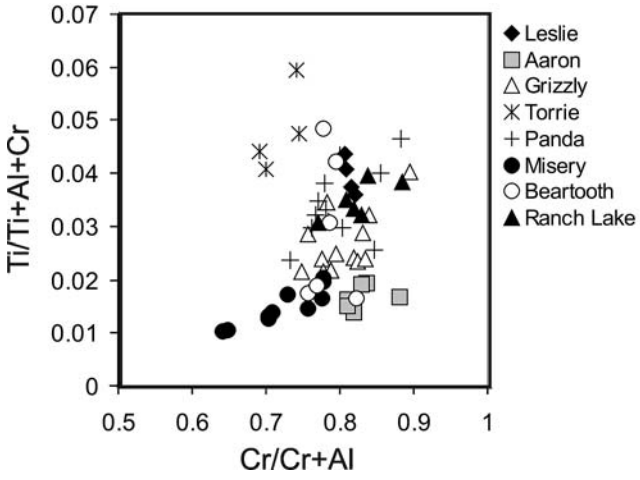

Fig. 8 Composition of aluminous magnesian chromite inclusions in olivine phenocrysts from the eight Lac de Gras kimberlites. The plot shows that chromites from different kimberlites differ in Cr- and Ti- content

Interestingly, our data show a negative correlation between the grade of a pipe (carats /tonne) and the fO_2 of the melt (Fig. 10). The grade is a general parameter and depends on a great variety of factors that include how diamondiferous the mantle source is, the mantle processes that might influence diamond presence or appearance, the sampling of the mantle by kimberlite and the properties of the kimberlite melt. The correlation indicates that magma redox may be important for the character of diamonds recovered from a kimberlite and deserves closer investigation.

To test the influence of conditions in kimberlite melt on diamond preservation we also examined the Ranch Lake kimberlite, which contains a good suite of "diamond" indicator minerals, implying sampling of a diamondiferous source, but nevertheless has a low diamond grade (Cookenboo 1996). The high oxidation state of this kimberlite (Fig. 7, Table 5) indicates that this parameter can play an important role in diamond preservation.

The resorption of octahedron to form THH may greatly influence the diamond volume and resultant grade of a pipe. Our data shows, however, that resorption increases with T, and that diamond grade decreases with increasing fO_2. Furthermore, the degree of resorption and grade do not necessarily correlate. For example, the Misery kimberlite has the highest grade, yet contains significantly more resorbed stones than Panda (Tables 1, 2).

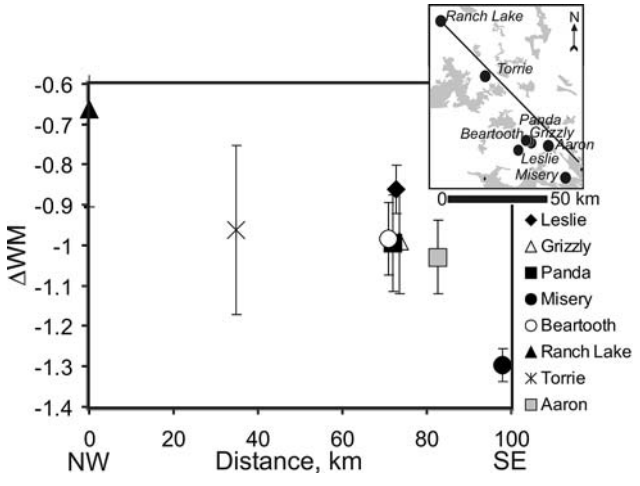

Fig. 9 Change in fO_2 of kimberlites shown relative to WM buffer (log fO_2 sample–fO_2WM buffer at P and T)) from NW to SE in the Lac de Gras area. Note the general reduction of kimberlite melt in the SE direction. The distances are given on the *line* shown on the insert in the *upper right corner*

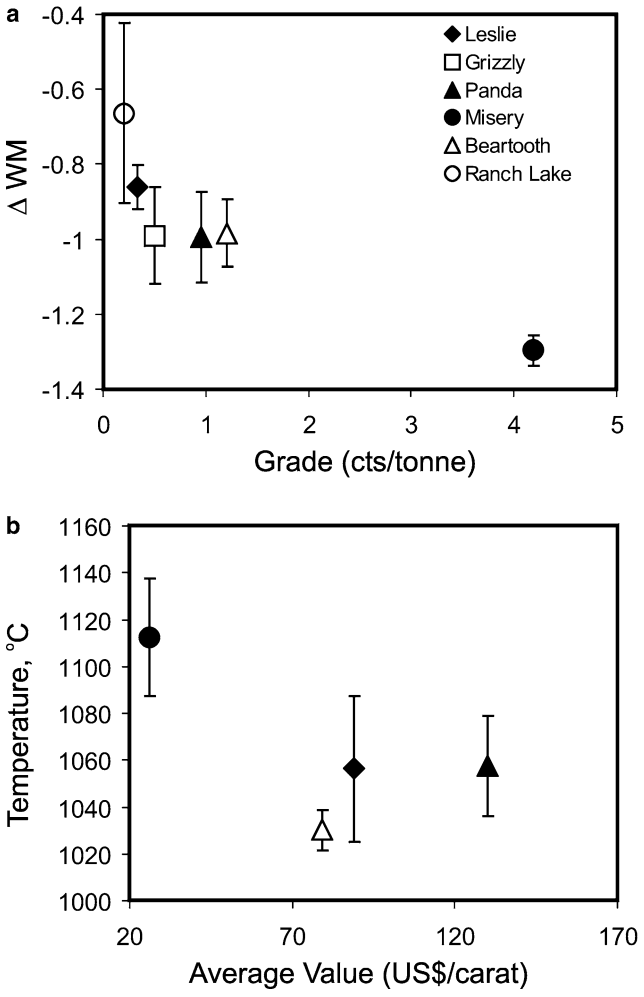

Fig. 10 Average values of fO_2 shown in Δ WM units versus diamond grade of a kimberlite (carats/tonne). The *error bars* are 1 SD. Diamond grades for Ekati pipes are from Natural Resources of Canada (http://www.nrcan.gc.ca/mms/cmy/content/1998/05.pdf) and for Ranch Lake from Cookenboo (1996)

The relative importance of events in the mantle or magmatic resorption is not known. As a result, the relationship between the degree of resorption and diamond grade may be very complex and partly reflect the history of the diamonds in both the mantle and the kimberlite. Conversely, there is also a possibility that the higher proportion of THH may indicate a lower degree of resorption. In a kimberlite, some diamonds included in xenoliths during emplacement are never exposed to interaction with the melt and remain unresorbed. The stones that are released from a xenolith react with melt, and in reactive media will be completely destroyed, resulting in a high O/THH ratio but low grade. In a less-reactive melt, the liberated diamonds are only partially dissolved and preserved as THH, resulting in low O/THH ratio but high grade. For stones released from xenoliths, more reactive kimberlites will have a higher proportion of THH amongst small diamonds, whereas less-reactive kimberlites will have O/THH ratio approximately similar in all size categories. In Panda and Beartooth, the O/THH ratio decreases towards the small diamonds, while in Misery it is approximately constant. Thus, there is a possibility that Panda and Beartooth diamonds underwent stronger dissolution than those at Misery, and in this case, the degree of resorption may be influenced by the oxidation state of the kimberlite magma.

The T dependence of diamond dissolution kinetics in kimberlite melts is well known from experiments. Kinetic data (Kozai and Arima 2003) show that a change in T from 1000°C to 1100°C results in threefold increase in resorption (in mm/h). Diamond oxidation in gases at controlled fO_2 can provide a proxy for diamond dissolution in melts with variable fO_2 (Evans and Phaal 1961;Cull and Meyer 1986; Sonin et al. 2000). Experimental data by Sonin et al. (2000) show that at fO_2 and T calculated for olivine–chromite kimberlite assemblages (carbon–carbon oxide fO_2 buffer and 1,100°C), change in 1 log unit fO_2 results in more than eight times faster diamond oxidation. Thus, even small difference in fO_2 of kimberlite melt may produce a notable difference in diamond grade of the pipe. This is confirmed by more recent data on the influence of fO_2 on diamond dissolution kinetics in kimberlite melts (Kozai and Arima, unpublished data).

Types of resorption produced by kimberlites

Some diamonds show a complex superposition of various dissolution features produced at different times (Fig. 4a). Diamond oxidation in experiments at different conditions (burning in air, dissolution in melts at variable T and P) produce similar surface features, some of which also develop during diamond growth (e.g. Afanasiev et al. 2000). Thus, it is usually not possible to distinguish resorption developed in the mantle from dissolution in a kimberlite melt; the appearance of a diamond may be a combination of both. A group of diamonds resided within the same domain would possibly share similar properties (degree of plastic deformation, impurities, nitrogen content and aggregation state) and undergo the same dissolution events. On the other hand, diamonds with identical properties, but that resided in the different parts of the mantle, may show similar behaviour when resorbed in kimberlite. Variations in the amount and distribution of defects within the diamond structure may result in different responses to resorption (Mendelssohn and Milledge 1995). All these factors complicate our understanding of the influence of kimberlite crystallization conditions on the character of resorption in different diamond parcels. By examining any possible correlations between different types of resorption, and diamond properties and degree of resorption, we use the Lac de Gras diamond data to get a better understanding on what type of resorption could have occurred in the kimberlite, as opposed to in the mantle.

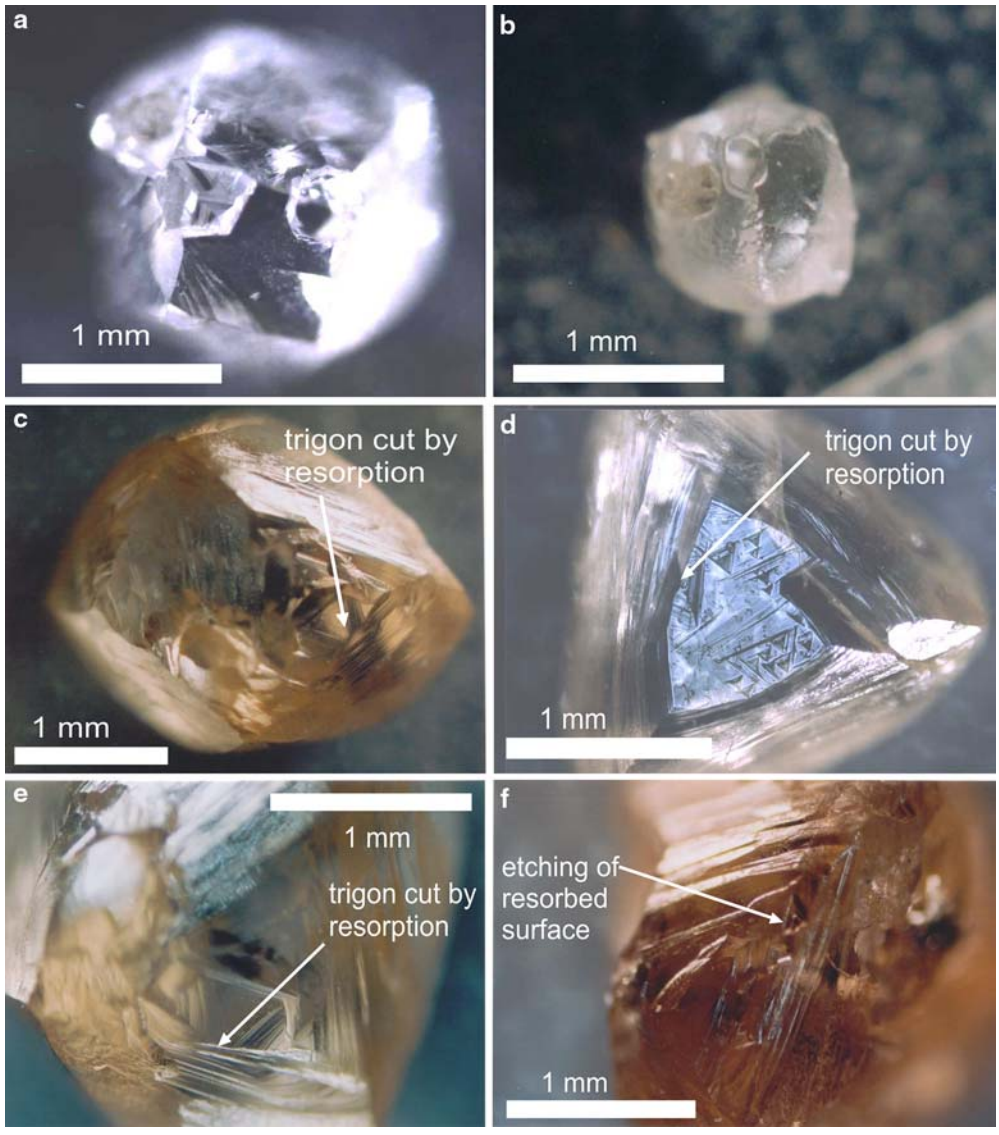

Fig. 11 Diamond photographs showing relationship between different dissolution forms: **a** Simultaneous formation of trigon and square pits. **b** Non-etched remnant of octahedral face on a diamond completely rounded by resorption. **c–e** Significantly resorbed octahedral diamonds with trigon pits cut by ditrigonal layers developed during resorption. **f** Trigon pits developed on a previously resorbed surface

Relationships between dissolution forms

The proportion of stones with different types of surface dissolution features vary between the five Lac de Gras pipes (Fig. 6). The correlation between etching and rutting processes agrees with their simultaneous development in experiments. The relationship between trigon and square pits is usually not obvious because the trigons and squares develop in the (111) and (100) directions, respectively, in some cases forming simultaneously (Fig. 11a). On the contrary, frosting shows no connection with the development of etch pits (Fig. 6) consistent with its development at a later stage of kimberlite emplacement where different parameters, possibly local conditions during emplacement, may play an important role.

In experiments (Kozai and Arima 2003) the resorption of octahedral faces is usually accompanied by the development of trigon and hexagon pits. Nevertheless, in the diamond parcels from this study, some of the significantly resorbed stones have remnants of flat octahedron faces without any etch pits (Fig. 11b). Moreover, there is no correlation between the resorption and etching. We calculated the proportion of stones with etch pits in the (111) direction in variously resorbed diamond groups (Fig. 12). The highest proportion of etched stones was recorded in the least resorbed parcels (Panda and Beartooth). Furthermore, within each kimberlite etching generally decreases with increasing resorption. The exception is the unresorbed groups with the lowest etching. These diamonds probably never experienced mantle resorption and were protected, perhaps in xenoliths, whilst in kimberlite melt. The low etching recorded in THHs, on the other hand, may be due to little preservation of the octahedron face (111) where the trigon and hexagon pits are formed on a diamond.

The multi-stage character of etching and resorption can be seen on individual diamonds (Figs. 4a, 11c–f).

Some of the trigon pits present on (111) faces are cut by ditrigonal layers formed during resorption in the (101) direction (Fig. 11c–e). The resorption therefore either postpones the etching or develops simultaneously. On the contrary, other trigons (Fig. 11f) were formed on previously resorbed surfaces clearly postponing resorption.

The lack of a positive correlation between etching and the degree of resorption in all five kimberlites indicate that these two processes do not accompany each other in every dissolution event and that each may be affected by different parameters. The total proportion of stones with various surface features produced by etching may therefore be more informative of the degree of diamond dissolution in kimberlite melt than the proportion of resorbed stones, which tend to be the product of resorption in both the kimberlite and the mantle.

Correlation of diamond properties and resorption

Internal diamond properties such as hydrogen and nitrogen content, defect aggregation state and plastic deformation are thought to influence resorption (Mendelssohn and Milledge 1995). Indeed, the most resorbed Lac de Gras diamond parcels (e.g. Misery and Jay) have the highest proportion of brown stones. Because brown colour is generally attributed to incipient graphitization produced during plastic deformation (Urusovskaya and Orlov 1964; Robinson et al. 1989), the presence of these defects in the diamond structure may result in the susceptibility of brown stones to destruct through dissolution (A. Afanasiev, personal communication, 2003). The fracturing of diamonds will also accelerate resorption.

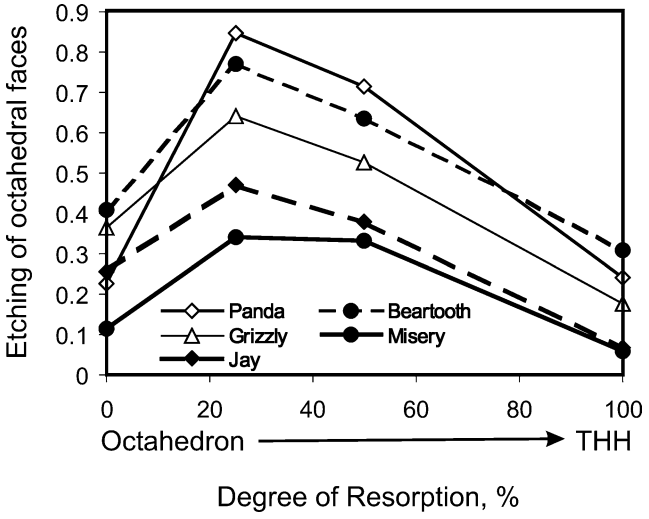

Fig. 12 Proportion of stones with trigon and hexagon pits in octahedral diamonds with different degrees of resorption. Degree of resorption shows percentage of octahedral faces resorbed (0%, unresorbed octahedron; < 50%, THH). Note the lack of a positive correlation between resorption of primary octahedron and development of etch pits

We made an attempt to evaluate the effect of diamond colour and fractures on the presence and the extent of some dissolution forms for the five Lac de Gras diamond parcels.

The degree of resorption (O/THH), and the presence of etch pits, ruts and frosting were examined as a function of colour (colourless to brown stone ratio, W/Br) and of the amount of internal fractures and cracks (Fig. 13). The Panda and Beartooth kimberlites have high O/THH and W/Br, but for the three pipes with low O/THH and W/Br ratios, there is no positive correlation between these two parameters. This suggests that differences in colour cannot explain the observed diversity of diamond dissolution characteristics in the five parcels. The presence of trigon etch pits, on the other hand, gradually increases in diamond groups having more brown stones (Fig. 13). This correlation is even stronger for the development of frosting. Neither forms of dissolution correlate with the amount of diamond fractures.

Conclusions

We show the fO_2 of kimberlite magmas determined from Ol–Sp oxygen barometry to be 2.8–4.4 log units below the NNO buffer. The T–fO_2 values for individual kimberlite pipes in the Lac de Gras area form trends showing more reducing conditions with decreasing T. There are significant variations in T–fO_2 values between the NW and SE clusters of kimberlites that are larger than uncertainties in the oxybarometry and correlate with substantial differences in the diamond populations (Afanasiev et al. 2000). The fO_2 decreases and crystallization T increases from the NW to SE cluster, whereas within the NW cluster Panda and Beartooth kimberlites have similar diamond populations and T– fO_2 values.

Various dissolution features in diamonds from the five Lac de Gras pipes correlate with T– fO_2 values for their kimberlite melts. The Misery kimberlite has the highest proportion of resorbed diamond forms (THH) and the highest crystallization T. The diamonds from more oxidized kimberlites (Panda and Beartooth) have more extensive development of surface dissolution features. There is no correlation between surface etching and volume resorption in our kimberlites. Development of etch features is more extensive in diamond groups with a higher proportion on brown (possibly plastically deformed) stones, whereas the degree of resorption does not follow this correlation. We suggest that the development of the surface etching mainly occurs in kimberlite melt and therefore is controlled by fO_2. Resorption, on the contrary, depends on the conditions in both the kimberlite and in the mantle source and its relationship with conditions in the magma are obscure.

The diamond grade of a kimberlite correlates negatively with its fO_2. Whether the range of observed fO_2 values represents variations in the oxidation/reduction processes in the kimberlite magmas, or were inherited

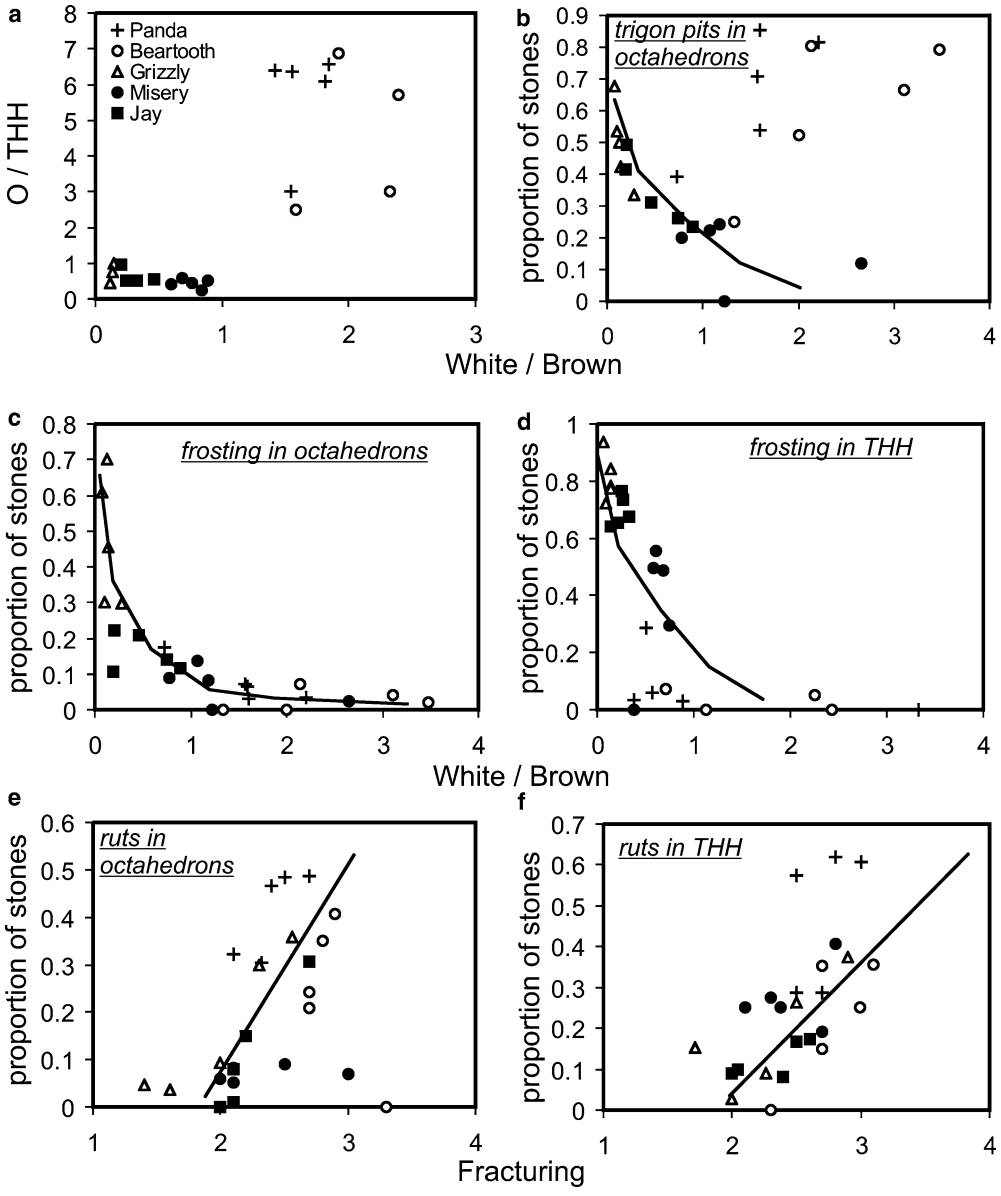

Fig. 13 Influence of diamond properties (colour and fractures) on the development of various dissolution forms in different diamond size groups for the Panda, Beartooth, Grizzly, Misery and Jay parcels. Only data for size groups with more than 100 stones are shown. **a** Degree of diamond resorption shown as octahedron to THH ratio (O/THH) versus colorless/brown stone ratio (W/Br) for the five kimberlites. **b–d** Higher proportion of stones with trigon pits (**b**) and frosting (**c, d**) in more brown diamond parcels. **e, f** Correlation between the presence of ruts on diamond surfaces and degree of internal fracturing. Fracturing ranges from 0 (no fractures present) to 5 (completely fractured stone) and was calculated as an average for each size group

from their mantle source is uncertain. The high fO_2 values determined for the Ranch Lake kimberlite, which has good suite of 'diamond indicator minerals' but low diamond grade, indicates that fO_2 of the magma plays a role in diamond preservation. The established correlations between T– fO_2 values of kimberlites and diamond resorption features suggest that conditions of the host kimberlite may notably influence the entrained diamonds. This opens up the possibility that given more data, oxybarometry obtained for kimberlite melts can be potentially used for diamond grade predictions.

Acknowledgements The diamond descriptions were completed by YF at BHP Billiton Diamonds Inc., whom we thank for generous access to drill core and diamonds, and for suggestions and permission to publish. We also thank T. Nowicki at Mineral Services Canada Inc., and M. Kopylova for providing some of the kimberlite samples, M. Kopylova and C. McCammon for the chromite 'Fe^{3+} standards', and M. Raudsepp for assistance with EMP analyses. We are grateful to J. Gurney for sharing his experience in diamond description, and M. Arima, C. Ballhaus and O. Navon for reviews. This research was supported by a Natural Sciences and Engineering Research Council of Canada Postgraduate Scholarship to YF and Discovery Grant to DC.

References

Afanasiev VP, Yefimova ES, Zinchuk NN, and Koptil VI (2000) Atlas of morphology of diamonds from Russian sources. SPC UIGGM, SB RAS

Arima M (1998) Experimental study of growth and resorption of diamond in kimberlitic melts at high pressures and temperatures. 7th International Kimberlite conference, pp 32–34

Ballhaus C, Berry RF, and Green DH (1991) High pressure experimental calibration of the olivine-orthopyroxene-spinel oxygen geobarometer: Implications for the oxidation state of the upper mantle. Contrib Miner Petrol 107:27–40

Chepurov AI, Khokhryakov AF, Sonin VM, and Pal'yanov YN (1985) Forms of dissolution of diamond crystals in silicate melts at high pressure. Doklady Akademii Nauk SSSR 285(1):212–216

Cookenboo H (1996) Ranch Lake kimberlite in the Central Slave Craton: the mantle sample. The Gangue 52:12–13

Creaser RA, Grütter H, Carlson J, and Crawford B (2004) Macrocrystal phlogopite Rb–Sr dates for the Ekati property kimberlites, Slave Province, Canada: evidence for multiple intrusive episodes in the Paleocene and Eocene. Lithos 76:399–414

Cull FA and Meyer HOA (1986) Oxidation of diamond at high temperature and 1 atm total pressure with controlled oxygen fugacity. 4th International Kimberlite conference, pp 377–379

Davis WJ, Kjarsgaard BA (1997) A Rb-Sr Isochron age for kimberlite from the recently discovered Lac de Gras Field, Slave Province, Northwest Canada. J Geology 105:503–509

Droop GTR (1987) A general equation for estimating Fe3+ concentrations in ferromagnesian silicates and oxides from microprobe analyses, using stoichiometric criteria. Min Mag 51:431–435

Edgar AD, Arima M, Baldwin DK, Bell DR, Shee SR, Skinner EMW, Walker EC (1988) High-pressure–high temperature melting experiments on a Sio2 poor, CaO-rich aphanitic kimberlite from the Wesselton mine, Kimberley, South Africa. Am Miner 73:524–533

Evans T, Phaal C (1961) The kinetics of the diamond–oxygen reaction. Conference on Carbon, pp 7–153

Fedortchouk Y, Canil D (2004) Intensive variables in kimberlite magmas, Lac de Gras, Canada and implications for diamond survival. J Petrol 45: 1725–1745

Fipke CE, Gurney JJ, Moore RO (1995) Diamond exploration techniques emphasising indicator mineral geochemistry and Canadian examples. Geol Surv Canada Bull 423:1–86

Frost B (1991) Introduction to oxygen fugacity and its petrologic importance. In: Lindsley DH (ed) Oxide minerals: petrologic and magnetic significance, Rev Miner 25. Min Soc America, pp 1–9

Gurney JJ, Hildebrand PR, Carlson JA, Fedortchouk Y, Dyck DR (2004) The morphological characteristics of diamonds from the Ekati property, Northwest Territories, Canada. Lithos 77:21–38

Harris JW, Vance ER (1974) Studies of the reaction between diamond and heated kimberlite. Contrib Miner Petrol 47:237–244

Holland TJB, Powell R (1998) An internally consistent thermodynamic data set for phases of petrological interest. J Metam Geol 16:309–343

Khokhryakov AF, Palyanov YN (1990) Morphology of diamond crystals dissolved in water-containing silicate melts. Mineralogicheskiy Zhurnal 12:14–23

Kozai Y, Arima M (2003) Diamond dissolution in kimberlite and lamproite melts at deep crustal conditions. 8th International Kimberlite conference

Lockhart G, Grutter H, Carlson JA (2004) Temporal, geomagnetic and related attributes of kimberlite magmatism at Ekati, Northwest Territories, Canada. Lithos 77:665–682

McCammon C, Kopylova MG (2004) A redox profile of the Slave mantle and oxygen fugacity control in the cratonic mantle. Contrib Mineral Petrol 148:55–68

Mendelssohn MJ, Milledge HJ (1995) Morphological characteristics of diamond population in relation to temperature-dependent growth and dissolution rates. Int Geol Rev 37:285–312

Mitchell RH (1986) Kimberlites: Mineralogy, geochemistry, and petrology. Plenum Press, New York, 660 p

Nassichuk WW, McIntyre DJ (1995) Cretaceous and tertiary fossils discovered in kimberlites at Lac de Gras in the Slave Province, Northwest territories. In: Interior plains and Arctic Canada Current Res - Geol Surv Canada. pp 109–114

O'Neill H, Wall VJ (1987) The olivine-orthopyroxene-spinel oxygen geobarometer, the nickel precipitation curve, and the oxygen fugacity of the Earth's upper mantle. J Petrol 28:1169–1191

Pal'yanov YN, Khokhryakov AF, Borzdov YM, and Sokol AG (1995) Diamond morphology in growth and dissolution processes. 6th International Kimberlite conference

Pell JA (1997) Kimberlites in the Slave Craton, Northwest Territories, Canada. Geosci Canada 24:77–90

Pouchou JL, Pichoir F (1985) PAP $\phi(\rho Z)$ procedure for improved quantitative microanalysis. Microbeam Analysis 104–106

Robinson DN, Scott JA, Neikerk AV, Anderson VG (1989) The sequence of events reflected in the diamonds of some southern African kimberlites. In: Ross J (ed) Kimberlites and related rocks, vol 2, no 14. Geological Society of Australia, Sydney, NSW, pp 990–1000

Sonin VM, Fedorov II, Pokhilenko LN, Pokhilenko NP (2000) Diamond oxidation rate as related to oxygen fugacity. Geol Ore Deposits 42:549–556

Sonin VM, Zhimulev EI, Afanas'ev VP, Chepurov AI (2002) Genetic aspects of the diamond morphology. Geology of Ore Deposits 44:291–299

Sunagawa I (1984) Morphology of natural and synthetic diamond crystals. In: Sunagawa (ed) Material science of the Earth's interior, pp 303–330

Taylor WR, Bulanova G, Milledge HJ (1995) Quantitative nitrogen aggregation study of some Yakutian diamonds: constraints on the growth, thermal, and deformation history of peridotitic and eclogitic diamonds. In: 6th International Kimberlite conference, pp 608–610

Urusovskaya AA, Orlov YL (1964) Nature of plastic deformation of diamond crystals. Doklady Akademii Nauk SSSR 154:112–115

Wood BJ, Virgo D (1989) Upper mantle oxidation state: ferric iron contents of lherzolite spinel by 57Fe Mössbauer spectroscopy and resultant oxygen fugacities. Geochim Cosmochim Acta 53:1277–1291

Yamaoka S, Kanda H, Setaka N (1980) Etching of diamond octahedrons at high temperatures and pressures with controlled oxygen partial pressure. J Mater Sci 15:332–336